Article

Structure Design and Optimization Algorithm of a Lightweight Drive Rod for Precision Die-Cutting Machine

Jing Wang [1,2]**, Xian Chen** [1,2] **and Yong Li** [1,2,*]

1   College of Mechanical and Electrical Engineering, Wenzhou University, Wenzhou 325035, China
2   Pingyang Institute of Intelligent Manufacturing, Wenzhou University, Wenzhou 325400, China
*   Correspondence: lyre@wzu.edu.cn

Abstract: In order to solve the problems of excessive elastic deformation and excessive inertia force existed in the drive mechanism of traditional die-cutting machine, a lightweight drive rod with full symmetrical structure is proposed as the main force bearing component of the drive mechanism based on the kinematics analysis. The elastic deformation and inertia force of the lightweight drive rod are verified by static simulation analysis, and show that the weight of the drive rod is significantly reduced under the same deformation conditions, the traditional one. Further compared with, taking the minimum elastic deformation and lightweight as the optimization objectives, the Non-dominated Sorting Genetic Algorithm-II (*NSGA-II*) is used to optimize the structural parameters of the drive rod. The results show that under the working conditions of 350 T die-cutting force and 125 r/min rotating speed, the elastic deformation of lightweight drive rod after structural optimization is smaller (the maximum deformation is 0.00988 mm) and the weight is lighter (27% less). The research data presented in this paper can be used as the theoretical basis for future research on die-cutting mechanism. The lightweight drive rod proposed in this study can be used in die-cutting devices with high die-cutting speed and high die-cutting accuracy.

Keywords: die-cutting machine; drive rod; lightweight; elastic deformation; optimization algorithm

1. Introduction

1.1. Application Field and Development Trend of Die-Cutting Machine

Nowadays, the packaging industry is developing rapidly in the world, and die-cutting plays an important role in the packaging industry. Die-cutting generally refers to a cutting process in the post-processing of printed matter. The process of die-cutting and indentation processing on the die-cutting machine is called die-cutting. Die-cutting machines are widely used in electronics, home appliances, communications, instruments, automobiles, medical devices, packaging and other industries [1–3].

Since the birth of die-cutting machine, the high-speed, high-precision, informatization and automation of die-cutting machine has been the main development direction, and its intellectualization and modularization are also the key development trend [4–6]. The die-cutting machine mainly includes three modules: paper feeding, die-cutting and paper receiving. The printing materials can be cut automatically and accurately through the cooperation of the three modules [7]. The drive mechanism is the key component of the die-cutting machine, and the research of its performance has been paid more and more attention by enterprises.

1.2. Research Direction and Achievements of Die-Cutting Machine

At present, the improvement of die-cutting machine mainly starts from two aspects: die-cutting speed and die-cutting accuracy. As the main part of die-cutting machine, the drive mechanism directly affects the speed and accuracy of die-cutting machine. Therefore, it is very important to analyze and study the drive mechanism of die-cutting machine [8].

In view of the drive mechanism of the die-cutting device, Lin et al. [9] used kinematics to analyze the drive mechanism, and then proposed a better material selection. Luo et al. [10] carried out elastic-plastic analysis on the drive mechanism of the die-cutting machine, summarized the stress and deformation of the mechanism under the maximum die-cutting force, and provided a reference for the future mechanism design. Yu et al. [11] analyzed the motion characteristics of the double-elbow bar mechanism of the die-cutting machine. Zhang et al. [12] used the loop method to analyze the motion of the double-elbow bar mechanism of the die-cutting machine, and optimized the drive mechanism. Lv [13] proposed a new type of fixed cam link intermittent motion mechanism to realize the intermittent paper feeding function of high-speed die-cutting machine. Xie et al. [14] carried out dynamic analysis on the double-elbow bar of the die-cutting machine, and obtained its motion characteristics and stress situation. Wei et al. [15] used numerical analysis method to analyze the mechanical mechanism of double-elbow bar, and designed experiments to verify the impact of vibration on die-cutting accuracy. Nu et al. [16,17] analyzed and studied the traditional double-elbow bar drive mechanism, proposed a new type of cam drive mechanism, and carried out mechanical analysis and material selection for the drive mechanism. Xiao [18] has carried out error analysis on the double-elbow bar mechanism, and obtained the result that the negative error of the bar length has little impact on the die-cutting accuracy.

According to the existing research results, most scholars mainly focus on the motion analysis and trajectory optimization of the double-elbow mechanism, and some scholars have optimized the material properties of the double-elbow mechanism.

Various studies have shown that when the die-cutting pressure increases, the drive parts involved in die-cutting device will have greater elastic deformation, resulting in a decline in die-cutting accuracy. At the same time, with the increase of the rotational speed of the die-cutting machine, the moving parts will generate greater inertia force, which will cause the speed of the drive mechanism to fluctuate, and the die-cutting accuracy of the die-cutting machine will inevitably decrease [19]. Therefore, ensuring the die-cutting accuracy of the die-cutting machine is the prerequisite for upgrading the die-cutting machine. In order to study how to improve the die-cutting accuracy, it is necessary to study the factors that affect the die-cutting accuracy. Summarizing the previous experience and the results of this study, it can be found that the tension of die-cutting materials and the operating accuracy of drive mechanism are the main influencing factors [20]. This study starts with the study of the part structure of the driven platform drive mechanism, and achieves the purpose of improving the die-cutting accuracy by optimizing the structure of the parts of the drive mechanism.

1.3. Research Objectives and Contents

According to the improvement direction of the die-cutting machine mentioned above, a lightweight drive rod of moving platform based on full symmetry structure is proposed to improve the die-cutting accuracy of drive mechanism. The multi-objective genetic algorithm is used to further optimize the structural parameters of the proposed lightweight drive mechanism components to obtain a dynamic platform drive rod with greater structural strength and lighter weight, which can achieve the function of smaller operating error. Dynamic simulation and prototype test are carried out on the drive rod to verify the accuracy of the optimal drive rod.

2. The Principle and Kinematics Analysis of the Drive Mechanism of Die-Cutting Device

2.1. The Composition and Principle of Die-Cutting Device Drive Mechanism

The double-elbow bar mechanism shown in Figure 1 is the most mainstream drive mechanism of the die-cutting device at the present stage, which is composed of mainly crankshaft 1, four power rods 2 and four groups of symmetrical drive rods 3. The drive mode is through the rotation of the crankshaft 1, the movement of the power rod 2 is driven,

and the drive rod 3 swings left and right under the drive of the power rod, thus driving the platform 4 to move up and down.
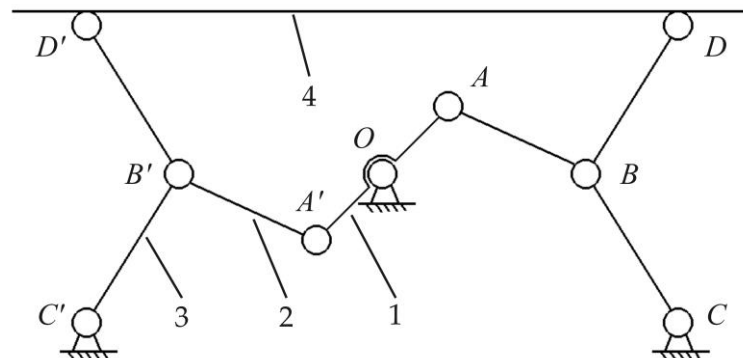

Figure 1. Schematic diagram of drive mechanism of die-cutting device. 1-crankshaft; 2-power rod; 3-drive rod; 4-moving platform.

2.2. Kinematics Analysis of Drive Mechanism of Die-Cutting Device

When operating at high speed, it is necessary to obtain the inertia force and moment of inertia of the drive rod through the kinematic analysis of the drive mechanism, which provides a prerequisite for the subsequent structural parameter optimization and dynamic simulation verification.

Considering that the drive mechanism of the moving platform is a symmetrical structure, only one side of the drive mechanism is taken as the analysis object in the kinematics analysis. According to the research results of other scholars [21–24], the lower drive rod of BC in Figure 1 is the most stressed part. Due to assembly restrictions, the upper drive rod of BD and the lower drive rod of BC must be the same size. Therefore, it is sufficient to analyze the drive rod with the greatest stress. In this paper, the lower drive rod of BC on one side of the drive mechanism is selected as the final analysis object. To determine the inertial force of the drive rod, it is necessary to analyze the motion of the connecting rod and calculate the speed and acceleration of the connecting rod.

According to the assembly relationship of crank, power rod and drive rod, its motion diagram can be established, and the force vector diagram of drive rod can be drawn according to the diagram (as shown in Figure 2). From the closed vector polygon OABCD, it can be obtained [25]:

$$\vec{l_1} + \vec{l_2} = \vec{l_5} + \vec{l_4} + \vec{l_3} \tag{1}$$

Among them: l_1, l_2, l_3, l_4, l_5 are the lengths of OA, AB, BC, CD, DO.
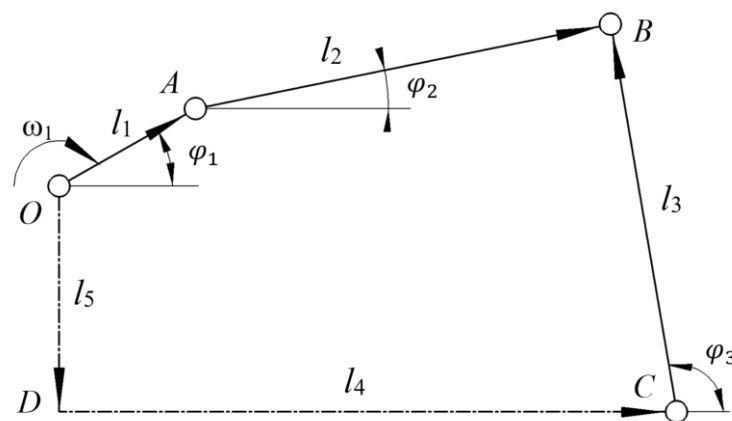

Figure 2. Vector relationship of the drive rod.

By projecting Formula (1) onto the coordinate axis, the position equation of the part can be obtained:

$$l_1 cos\varphi_1 + l_2 cos\varphi_2 = l_4 + l_3 cos\varphi_3$$
$$l_1 sin\varphi_1 + l_2 sin\varphi_2 = -l_5 + l_3 cos\varphi_3 \tag{2}$$

The solution can be obtained:

$$\varphi_2 = arcsin\frac{C_1}{\sqrt{A_1^2 + B_1^2}} - arctan\frac{B_1}{A_1}$$

$$\varphi_3 = arcsin\frac{C_2}{\sqrt{A_2^2 + B_2^2}} - arctan\frac{B_2}{A_2}$$

In the formula:

$$A_1 = -2l_5l_3 - 2l_1l_3 sin\varphi_1$$

$$A_2 = 2l_1l_2 sin\varphi_1 + 2l_2l_5$$

$$B_1 = 2l_4l_3 - 2l_1l_3 cos\varphi_1$$

$$B_2 = 2l_1l_2 cos\varphi_1 - 2l_1l_4$$

$$C_1 = l_2^2 - l_3^2 - l_5^2 - l_4^2 - l_1^2 - 2l_1l_5 sin\varphi_1 + 2l_1l_4 cos\varphi_1$$

$$C_2 = l_3^2 - l_1^2 - l_2^2 - l_4^2 - l_5^2 - 2l_1l_5 sin\varphi_1 + 2l_1l_4 cos\varphi_1$$

Here, take $l_1 = 45$ mm, $l_2 = 217$ mm, $l_3 = 178$ mm, $l_4 = 280$ mm, $l_5 = 185.3$ mm. The position change information of the drive rod can be calculated by substituting the rod length parameter into Formula (2) (see Figure 3):
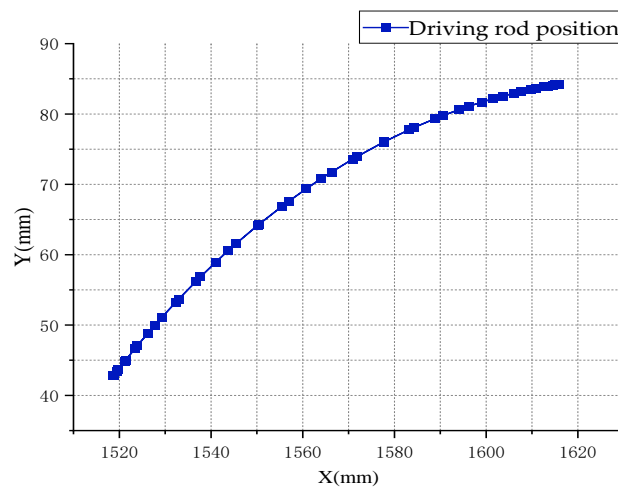

Figure 3. Position of drive rod.

Among them: the abscissa represents the position of the drive rod vertex in the "X" axis direction on the operation plane, and the ordinate represents the position of the drive rod vertex in the "Y" axis.

By taking the first derivative of Formula (2) with respect to time, the angular velocity equation can be obtained:

$$l_1\omega_1cos\varphi_1 + l_2\omega_2cos\varphi_2 = l_3\omega_3cos\varphi_3$$
$$l_1\omega_1sin\varphi_1 + l_2\omega_2sin\varphi_2 = l_3\omega_3sin\varphi_3 \tag{3}$$

The solution can be obtained:

$$\omega_2 = -\frac{l_1\omega_1sin(\varphi_3 - \varphi_1)}{l_2sin(\varphi_3 - \varphi_2)}$$

$$\omega_3 = \frac{l_1\omega_1sin(\varphi_1 - \varphi_2)}{l_2sin(\varphi_3 - \varphi_2)}$$

In the formula: ω_1, ω_2, ω_3 are the angular velocities of *OA*, *AB* and *BC*, respectively.

Here take $\omega_1 = 125$ r/min. The angular velocity change information of the drive rod can be calculated from the Formula (3) (Figure 4):
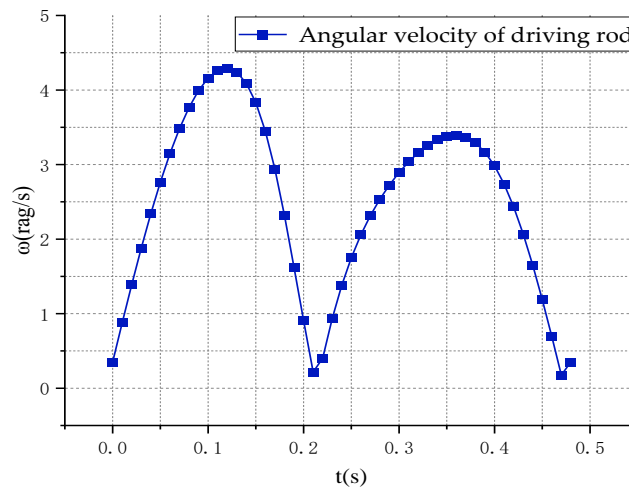

Figure 4. Angular velocity of drive rod.

The angular acceleration equation of the drive rod can be obtained by calculating the first derivative of Formula (3) to time.

$$-l_1\omega_1^2sin\varphi_1 + l_2a_2cos\varphi_2 - l_2\omega_2^2sin\varphi_2 = l_3a_3cos\varphi_3 - l_3\omega_3^2sin\varphi_3$$
$$l_1\omega_1^2cos\varphi_1 + l_2a_2sin\varphi_2 + l_2\omega_2^2cos\varphi_2 = l_3a_3sin\varphi_3 + l_3\omega_3^2cos\varphi_3 \tag{4}$$

The solution can be obtained:

$$a_2 = \frac{l_4\omega_4^2 - l_1\omega_1^2cos(\varphi_1 - \varphi_3) - l_2\omega_2^2cos(\varphi_2 - \varphi_3)}{l_2sin(\varphi_2 - \varphi_3)}$$

$$a_3 = \frac{l_2\omega_2^2 + l_1\omega_1^2cos(\varphi_1 - \varphi_2) - l_3\omega_3^2cos(\varphi_3 - \varphi_2)}{l_3sin(\varphi_3 - \varphi_2)}$$

In the formula: a_2 and a_3 are angular acceleration of *AB* and *BC*.

The angular acceleration change information of the drive rod can be calculated from Formula (4) (Figure 5):
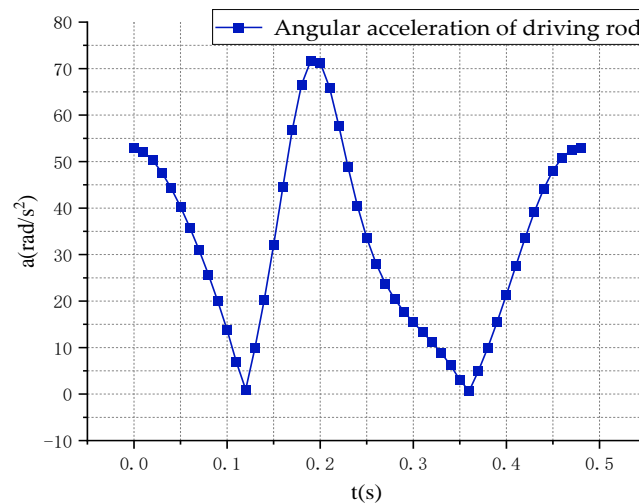
Figure 5. Angular acceleration of drive rod.

After calculating the angular acceleration of the driving rod, the inertia force of the driving rod can be obtained. Since the subsequent calculation in this paper only needs the strength of inertia force and moment, the inertia force and moment of inertia are calculated in scalar. Therefore, the strength of the inertia force and torque of the drive rod can be calculated by Formulas (5) and (6) [25].

$$F' = ma_i \tag{5}$$

$$J = mr_T^2 \tag{6}$$

In the formula: "m" is the weight of the drive rod, "r_T" is the rotation radius of the drive rod.

From the above analysis results, the drive rod has three times of rapid change of angular velocity and direction in one operation cycle, and the speed is large (Figure 4). In Figure 5, the acceleration of the drive rod is very large and the acceleration time is very short. Therefore, it can be concluded that the impact of the drive rod is very large, so the drive mechanism has high requirements for the rigidity and strength of the drive rod. From Formulas (5) and (6), it can be seen that the mass of the drive rod is positively related to its inertial force and moment of inertia. Therefore, the increase of the weight of the drive rod will inevitably lead to a significant increase in its inertial force and moment of inertia, which will add more additional loads to the drive rod. Therefore, the necessary condition to improve the performance of the drive mechanism is to increase the rigidity and strength of the drive rod and reduce its weight.

3. Design of a Lightweight Drive Rod Based on Fully Symmetrical Structure

3.1. Structural Characteristics and Shortcomings of Traditional Double-Elbow Bar Mechanism

In traditional double-elbow mechanisms, the drive rod has two common structures, as shown in Figures 6 and 7. The drive rod in Figure 6 is a solid structure that is mainly used for die-cutting machines with large cutting forces, this drive rod has the advantages of high compressive strength and convenient processing, but the disadvantage is low bending moment strength. This drive rod has a greater weight and is subjected to greater inertial forces during high-speed operation. Therefore, the vibration of the drive rod during high-speed operation is greater, resulting in lower driving accuracy (Figures 8 and 9). The hollow drive rod shown in Figure 7 is suitable for die-cutting machines with small cutting forces. This hollow drive rod has the advantages of high flexural strength, lightweight and material economy. Use ANSYS software (workbench 2021) to carry out static analysis on it, and apply die-cutting force component F_N on the upper circular surface of the drive rod, the lower round surface is supported by a cylinder. According to its mechanical analysis

results (Figures 10 and 11), the drive rod has a significant stress concentration, large strain and large elastic deformation during driving, resulting in its inability to operate normally under high die-cutting forces.
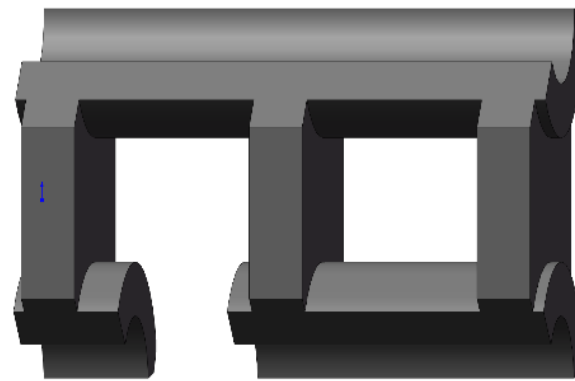

Figure 6. Solid drive rod model.

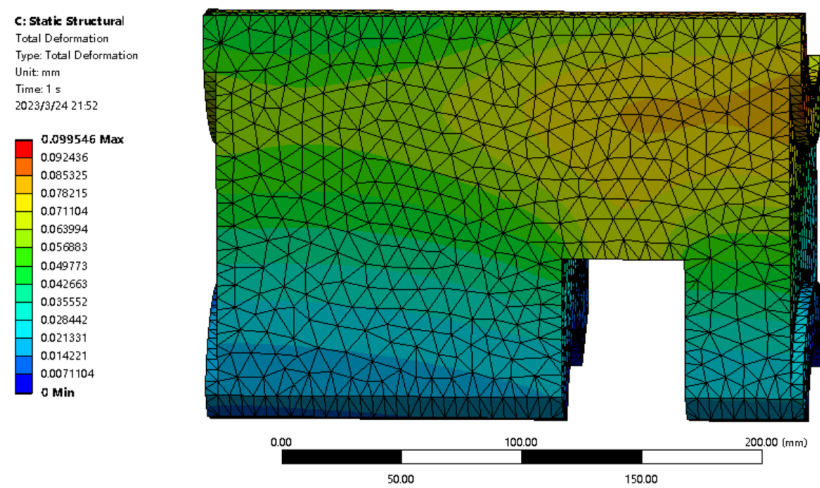

Figure 7. Hollow drive rod model.
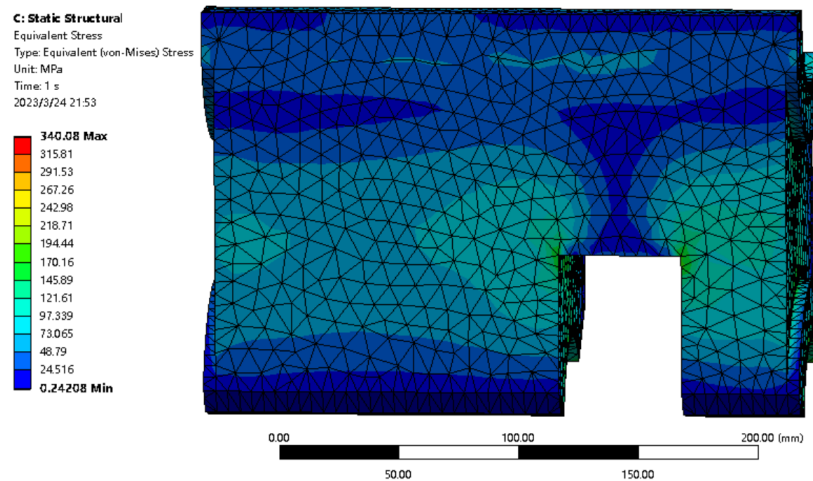

Figure 8. Deformation of solid drive rod.

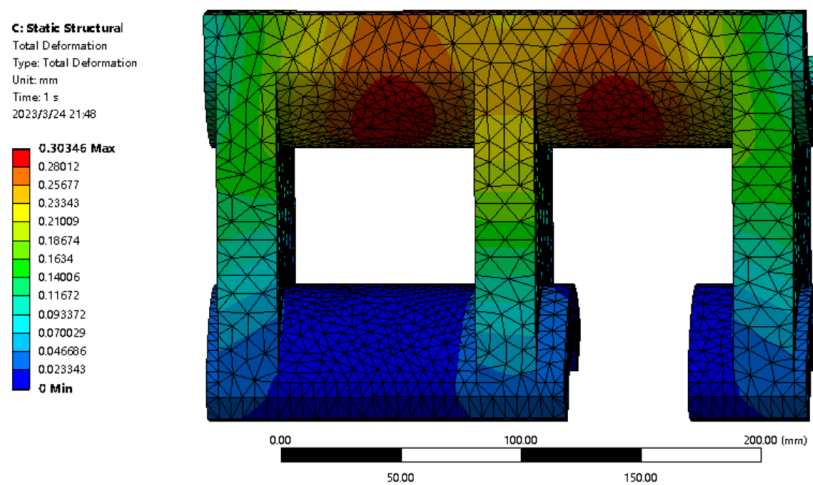**Figure 9.** Stress of solid drive rod.

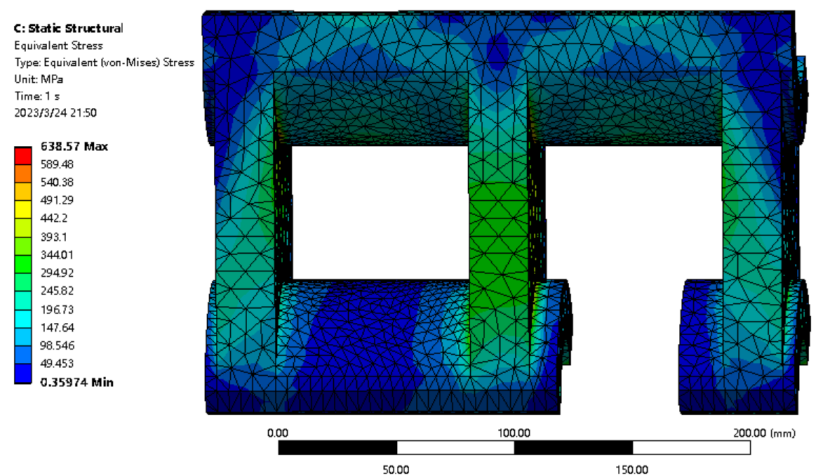**Figure 10.** Deformation of hollow drive rod.

Figure 11. Stress of hollow drive rod.

3.2. Performance Requirements of Drive Rod for High Precision Die-Cutting Device

According to the previous analysis, the respective performance defects of the two traditional drive rods restrict the improvement of die cutting accuracy. The reasons are summarized as follows: Firstly, the uneven stress distribution of the drive rod and the

low structural stiffness lead to large elastic deformation of the drive mechanism during operation; Secondly, due to the large mass of the drive rod, its inertia force during high-speed operation is large, resulting in large vibration of the drive mechanism. Therefore, future high-speed precision die-cutting machines have higher requirements for the drive rod, which requires higher strength under the same material and load, as well as lighter weight of the drive rod to reduce inertial impact. Ensure that the drive rod can withstand light and heavy load operating conditions in limited space. This study starts with the drive rod and proposes a new and more powerful drive rod to improve the accuracy of the die-cutting machine.

3.3. Scheme Design of Lightweight Drive Mechanism Based on Fully Symmetrical Structure

For the two traditional drive rod described above, this study proposes a new lightweight drive rod based on a fully symmetric structure (Figure 12). The structural shape of the drive rod was designed using the "I" pattern, and then, the stability of the drive rod structure was strengthened by symmetrically distributing three reinforcing ribs on the left and right sides. The lightweight drive rod has stronger compression and bending moment resistance, and is lighter in weight. The drive rod better solves the defects of large deformation and heavy weight existing in the above two types of drive rods.
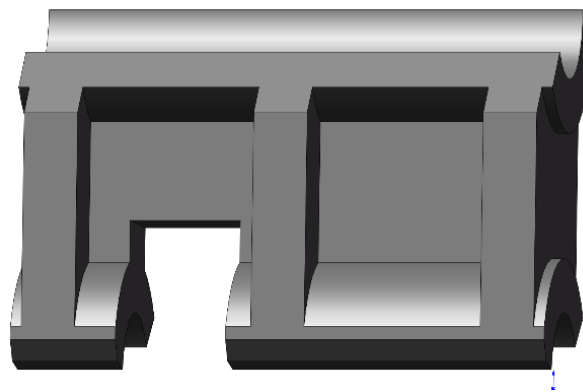

Figure 12. The lightweight drive rod based on fully symmetry structure.

3.4. Parameters Determination of Lightweight Drive Rod Based on Fully Symmetry Structure

Parameterize the lightweight drive rod according to its structural characteristics (Figure 13). In consideration of the structural characteristics of the drive rod, assembly space and operating space constraints, the design range of size parameters can be listed (see Table 1).
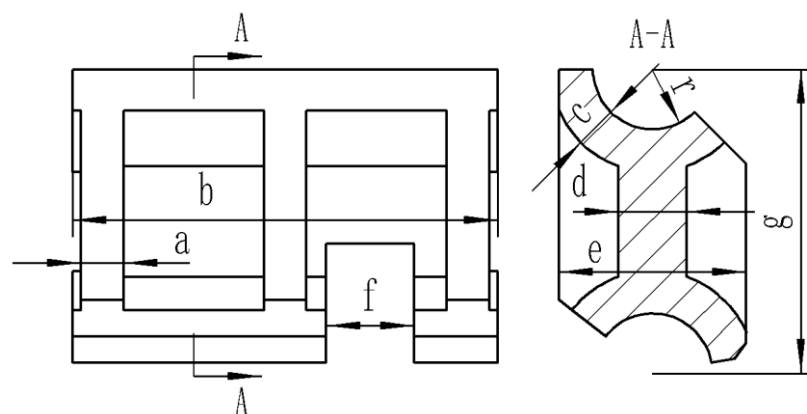

Figure 13. Structural parameters of lightweight drive rod.

Table 1. Design parameters range of the lightweight drive rod.

Parameter Name	a (mm)	b (mm)	c (mm)	d (mm)	e (mm)	f (mm)	g (mm)	r (mm)
Parameter range	$0 < a < \dfrac{b-10}{3}$	$3a + 10 < b < 260$	$0 < c < \dfrac{g-2r}{2}$	$0 < d < e$	$d < e \leq 2(r+c)$	$46 < f < \dfrac{b-10-3a}{2}$	178	35

The lightweight drive rod is designed for the 1060 mm × 760 mm die-cutting sheet, so it is limited by the transmission distance and mating components, and the two design parameters "g" and "r" are fixed values. Then, based on the range of the above design parameters, the specific values of each parameter are determined according to the mechanical design principles. First, determine the total width of the drive rod "b". Considering the reserved space for the operation of the drive rod and referring to the data of the traditional double-elbow bar, it is determined that b = 250 mm. Second, determine the thickness of the side reinforcement "a". There are three reinforcing ribs evenly distributed on the left and right sides of the lightweight drive rod. Based on the design principle of the reinforcing ribs and referring to the data of the traditional hollow double-elbow bar, it is determined that a = 25 mm. Third, determine the thickness of the rotating surface "c". According to the force magnitude of the drive rod, combined with the relationship between the force and strain of the material, and on the premise of ensuring the rigidity and strength requirements, it is determined that c = 25 mm. Fourth, determine the thickness "d" of the main support wall. The main support surface is mainly used to ensure the stability of the spatial structure during the movement of the drive rod, and its determined value is d = 40 mm. Fifth, determine the total width "e" of the stiffener. During operation, the stiffener mainly carries the torque of the drive rod. The greater the "e", the stronger the resistance to torque. Considering the reserved operating space, it is determined that e = 110 mm. Finally, determine the reserved slot width "f" of the drive rod. Without affecting the smoothness of operation, the smaller the value of "f", the better; so, it is determined that f = 51 mm. Summarize the final values of each design parameter based on the above parameter analysis (see Table 2).

Table 2. Design parameters of the lightweight drive rod.

Parameter Name	a (mm)	b (mm)	c (mm)	d (mm)	e (mm)	f (mm)	g (mm)	r (mm)
Parameter value	25	250	25	40	110	51	178	35

After completing the above parameter determination, the finite element analysis of the lightweight drive rod is shown in Figures 14 and 15. The results show that compared with traditional drive rod, the stress concentration and strain of lightweight drive rod has greatly improved under the same material and load.

Summarize the deformation and weight results of two conventional and lightweight drive rod (Table 3). The results show that the overall performance of the lightweight drive rod is superior to that of the traditional drive rod. In addition, better performance results can be further explored by optimizing drive rod parameters.

Table 3. Comparison of analysis results of three drive rods.

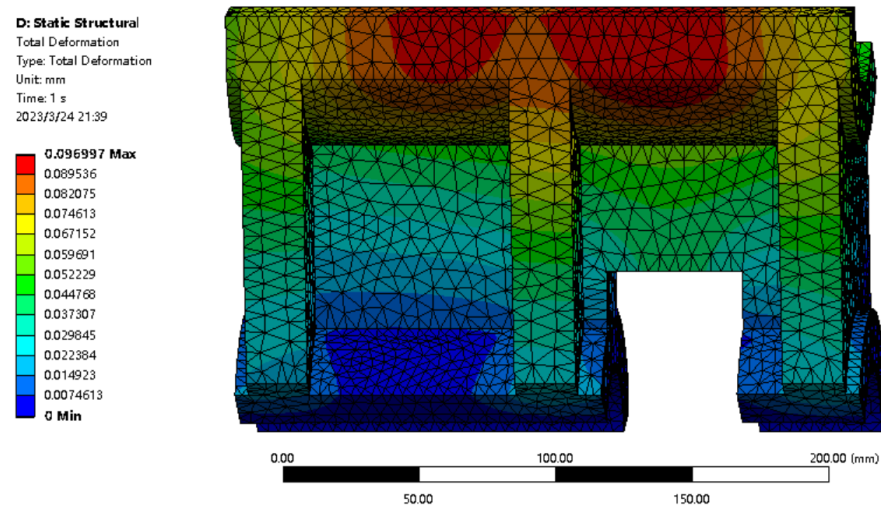| Parameters Name	Weight (kg)	Maximum Deformation (mm)
Solid drive rod	21.934	0.099
Hollow drive rod	13.152	0.303
Lightweight drive rod	15.861	0.096

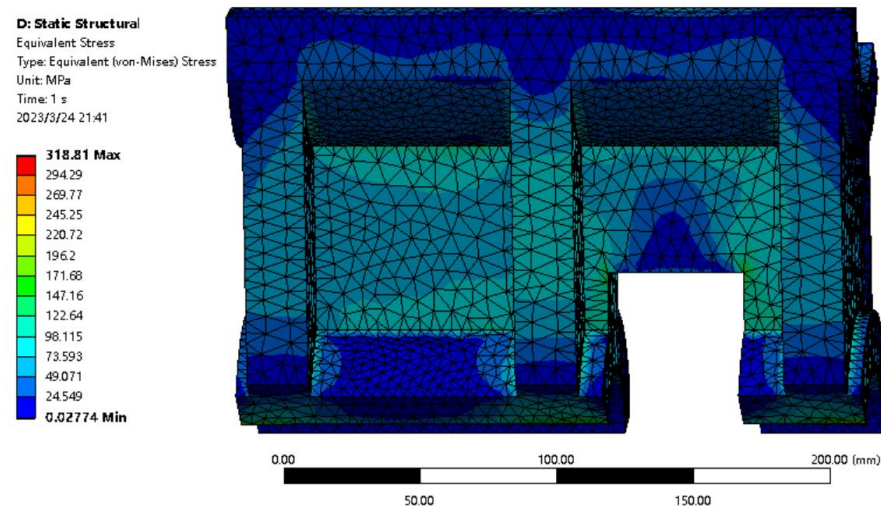**Figure 14.** Deformation of lightweight drive rod.

Figure 15. Stress of lightweight drive rod.

4. Parameter Optimization of the Lightweight Drive Rod Based on Fully Symmetrical Structure

On this basis, a multi-objective genetic algorithm can be used to further optimize the structural parameters of the drive rod to obtain better performance. The principle of optimization is to reduce the weight of the drive rod while ensuring that the strength and stiffness of the drive rod meet the requirements. This can not only reduce the deformation of the drive rod, but also reduce its weight, which can improve the problem of large vibration caused by large inertial forces. According to the structure of the drive rod, there are many parameters that affect the optimization goal, so it is necessary to establish a correct mathematical model.

4.1. Sensitivity Analysis of Optimization Parameters

There are many structural parameters for lightweight drive rod, and each parameter has a different impact on design goals. In order to facilitate the optimization process, sensitivity analysis should be conducted for each parameter, and those parameters that have little impact on the optimization goal should be eliminated before optimization.

The parameterized drive rod model is imported into ANSYS software, with variable parameters as input parameters, weight and elastic deformation as output targets. Sen-

sitivity analysis is performed on the variable parameters of the model using a sensitivity analysis module. The analysis results are shown in Figure 16.

After analyzing the sensitivity of each parameter, we can see from the results that the parameters that are relatively sensitive to the optimization goal include: the thickness of the stiffener "a", the total width of the drive rod "b", the wall thickness of the rotating surface "c", the thickness of the main support wall "d", and the total width of the stiffener "e". Therefore, the above five parameters are taken as design variables.
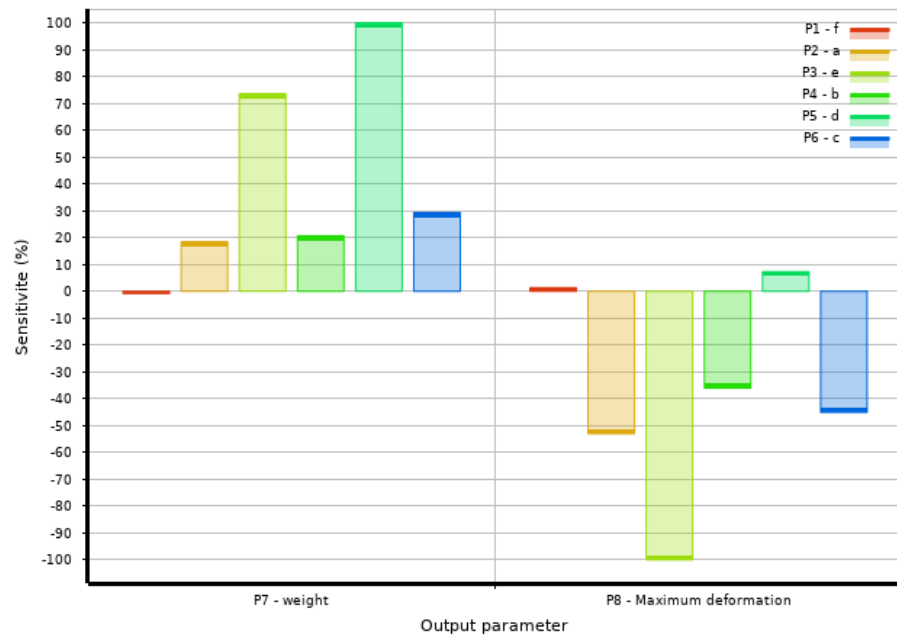

Figure 16. Result of parameters sensitivity analysis.

4.2. Determining the Target Function

According to the working conditions of the lightweight drive rod, after applying a corresponding force to it, it needs sufficient strength to ensure that the elastic deformation of the overall structure remains within a small range. In principle, the smaller the elastic deformation of the lightweight drive rod under working conditions, the better. Therefore, taking the elastic deformation of the driving rod in the force direction as the first optimization objective, a first objective function is established (Equation (7) [26]).

$$minf_1(X) = min\left(\frac{F_\sum L}{EA}\right) \tag{7}$$

where, "$F_\sum$" is the force on the drive rod; "L" is the length of the lightweight drive rod, namely the value of "b"; "E" is the elastic modulus of connecting rod material; and "A" is the cross-sectional area. According to the schematic diagram of the cross section of the lightweight drive rod shown in Figure 17, the calculation formula of "A" is:

$$A = 2 \times \frac{7\pi c^2}{4} + d(g - 2R) - 2 \times \left(\frac{\theta}{360}\pi R^2 - \frac{d(R-h)}{2}\right)$$

$$R = r + c$$

$$h = R - R\cos\theta$$

$$\theta = arccos\frac{2R^2 - d^2}{2R^2}$$

$$X = [x_1, x_2, x_3, x_4, x_5]^T = [a, b, c, d, e]^T$$

while ensuring the elastic deformation demand of the drive rod, the weight of the drive rod should be smaller. Therefore, taking the weight of the drive rod as the second optimization objective, a second objective function is established (Equation (8)):

$$min f_2(X) = min(\rho V) \tag{8}$$

where, "ρ" is the density of the lightweight drive rod; "V" is the volume of the lightweight drive rod. "V" can be calculated as follows:

$$V = 3a\left(eg - \frac{7\pi R^2}{4} - \frac{R^2}{2}\right) + (b - 3a)\left[\frac{7\pi c^2}{2} + d(g - 2R) - \left(\frac{\theta}{180}\pi R^2 - d(R - h)\right)\right]$$
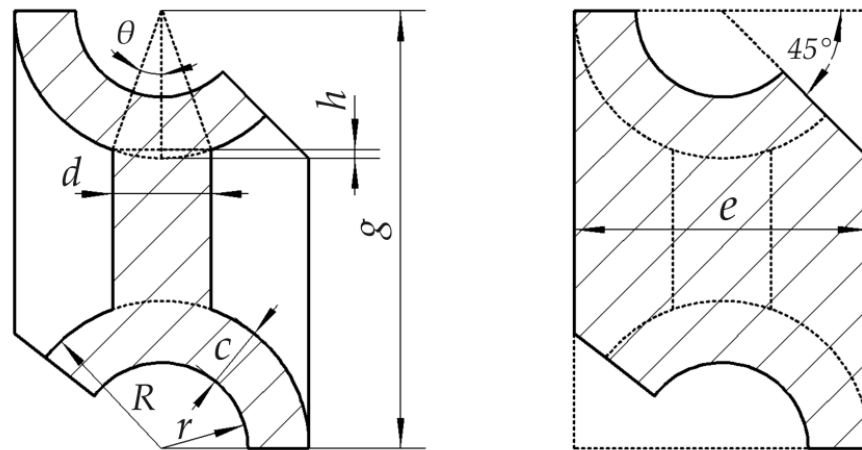

Figure 17. Cross-section of drive rod.

4.3. Determine the Constraints

Due to the limitations of the assembly space layout, the size of the drive rod needs to be set within a limited range, so, it is necessary to constrain the above design variables. Considering the structural characteristics of the drive rod, the constraint conditions for the above design variables are determined as follows:

$$0\,\text{mm} < a < \frac{b - 10}{3}$$

$$3a + 10 < b < 265\,\text{mm}$$

$$20.5\,\text{mm} < c < 27.5\,\text{mm}$$

$$0\,\text{mm} < d < e$$

$$d < e < 2(r + c)$$

The maximum positive force of the drive rod can be determined under a working environment with a maximum cutting force of 350 t and a maximum rotational speed of 125 r/min. Because there are four sets of drive rods, they are arranged in a rectangular shape. Four sets of driving rods jointly drive the operation of the mobile platform. The mobile platform moves up and down in a left and right swing manner, so during a period of time, one side of the mobile platform will bear all the mold cutting forces, that is, two sets of drive rods will bear a maximum mold cutting force of 350 t. According to the average distribution method, the maximum cutting force required to support a group of drive rods is F_N:

$$F_N = 1715\,\text{kN}$$

Due to the fact that the drive rod is a high-speed running part, it is necessary to consider its inertial force. According to Formula (5), the value of the inertial force of the drive rod can be obtained. Since this article is an analysis of the maximum force on the

drive rod, the maximum inertial force in the axial direction of the drive rod is selected as the value of F'_{max}. According to the distribution of the above die cutting force and inertial force, the external load constraint of the drive rod can be determined as follows (Equation (9)):

$$F_{\Sigma} = F_N + F'_{max} \tag{9}$$

4.4. Genetic Algorithm Optimization of Non-Dominated Sorting (NSGA-II)

NSGA-II algorithm is currently one of the most widely used multi-objective optimization algorithms. Compared with general genetic algorithms, *NSGA-II* algorithm has the characteristics of low complexity, good convergence of solution sets, and fast running speed. It uses a fast non dominant genetic algorithm to reduce computational complexity. Introduce elite strategies to prevent the loss of excellent populations during the evolution process, and use crowding comparison operators to ensure population diversity [27–29]. The optimization process is as follows (Figure 18):
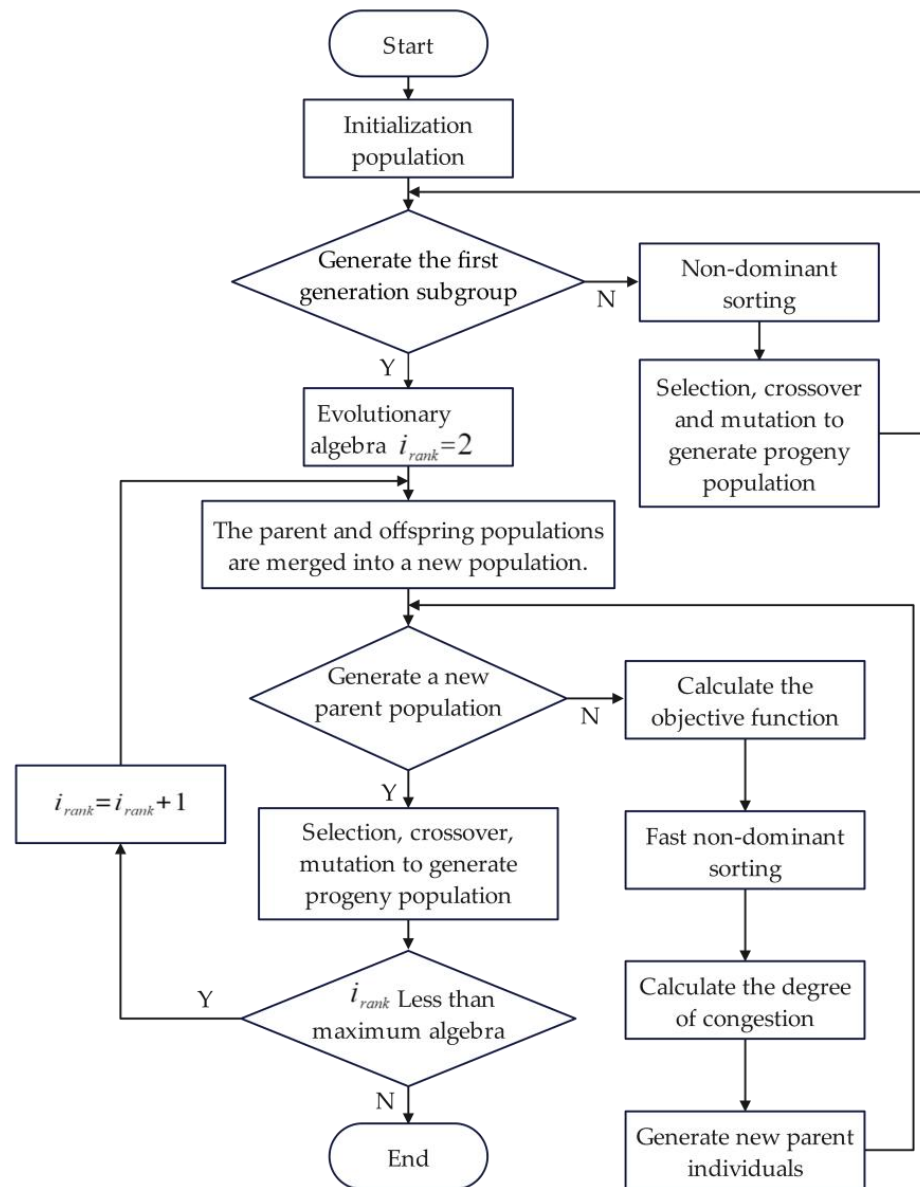

Figure 18. Optimization flow chart of *NSGA-II*.

4.4.1. Design of Fast Non-Dominant Sorting Operator

Firstly, find out the non-dominated solution set in the grope, and record it as the first non-dominated layer "F_1". Assign all its individuals a non-dominant order value $i_{rank} = 1$ (where "i_{rank}" is the non-dominant order value of individual "i"), and removed from the whole population. Then, the non-dominant solution set of the remaining population was further found, denoted as the second non-dominant rank layer "F_2" and the individuals were assigned the non-dominant rank value $i_{rank} = 2$. This is continued until the entire population is stratified and individuals within the same stratification have the same non-dominant order value "i_{rank}".

4.4.2. Design of Individual Crowded Distance Operator

The crowding distance of individual "i" is the distance between "$i + 1$" and "$i - 1$" of the two individuals adjacent to "i" in the target space, and its calculation steps are as follows:

1. The initialization distance of individuals in the same layer is represented by $L[i]_d$, let $L[i]_d = 0$;
2. The individuals in the same layer are sorted in ascending order according to the value of the m objective function;
3. To make the individuals on the sorting edge have a selection advantage, given a large number "M", let $L[0]_d = L[i]_d = M$;
4. For the individuals in the middle of the ranking, calculate the crowding degree distance:
$$L[i]_d = L[i]_d + (L[i+1]_m - L[i-1]_m) / \left(f_m^{max} - f_m^{min} \right)$$
5. For different objective functions, steps 2~4 are repeated to obtain the crowding distance "$L[i]_d$" of individual "i". By preferentially selecting individuals with larger crowding distances, the calculated results can be evenly distributed in the target space to maintain the diversity of the population.

4.4.3. Elite Strategy Selection Operator Design

The elite strategy is to keep good individuals in the parent generation directly into the child generation to prevent the loss of Pareto optimal solution obtained. The elite strategy selection operator optimizes the population "R_i" synthesized by parent "C_i" and child "D_i" according to three indexes to form a new parent population "C_{i+1}". Firstly, the scheme verification flag in the parent generation is eliminated as infeasible scheme. Secondly, according to the non-dominant order value "i_{rank}" from low to high, the whole species was placed into "C_{i+1}" successively, until the size of "C_{i+1}" exceeded the population size limit N when "F_j" was placed in a certain layer. Finally, "C_{i+1}" is continued to be filled according to the order of individual crowding distance in "F_j" from large to small until the population number reaches "N".

4.4.4. Optimization Calculation and Results of Non-Dominated Sorting Genetic Algorithm II

NSGA-II multi-objective genetic algorithm is used to optimize the mathematical model of the lightweight drive rod. The setting control of the algorithm was as follows: The weight of the two optimization objectives is 50%, the initial sample number generated by the population is 10,000, the crossover probability is 0.8, the mutation probability is 0.2, the sample number for each iteration is 5000, and the convergence stability percentage is set to 0.1. The convergence criteria can be obtained as shown in Figure 19.
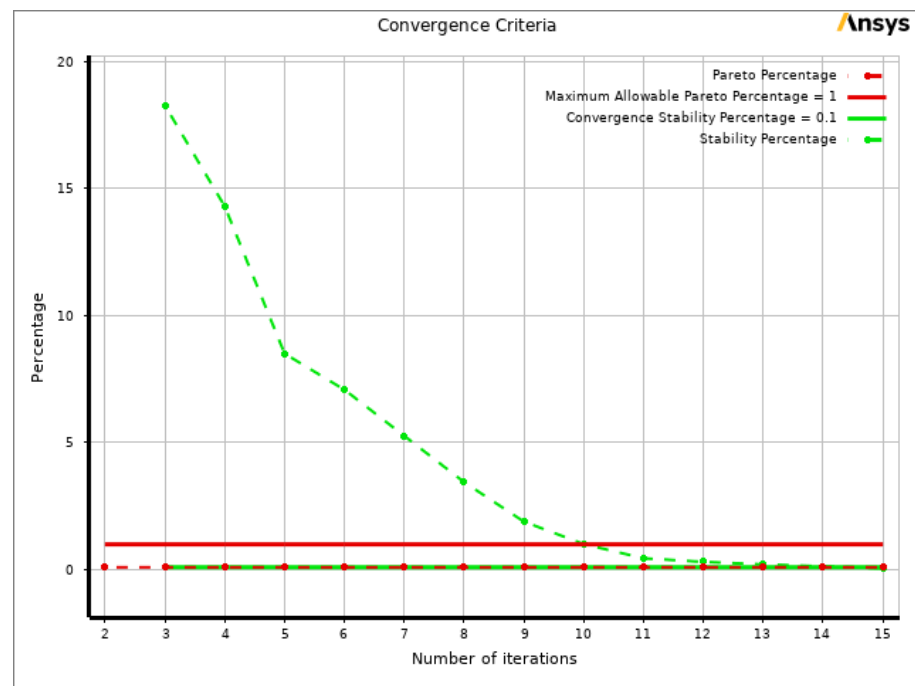
Figure 19. Convergence criteria.

This article uses Workbench to calculate the optimized mathematical model, record the parameters and targets, and according to the set convergence criteria, the convergence process of each parameter and target can be obtained (Figures 20–26).
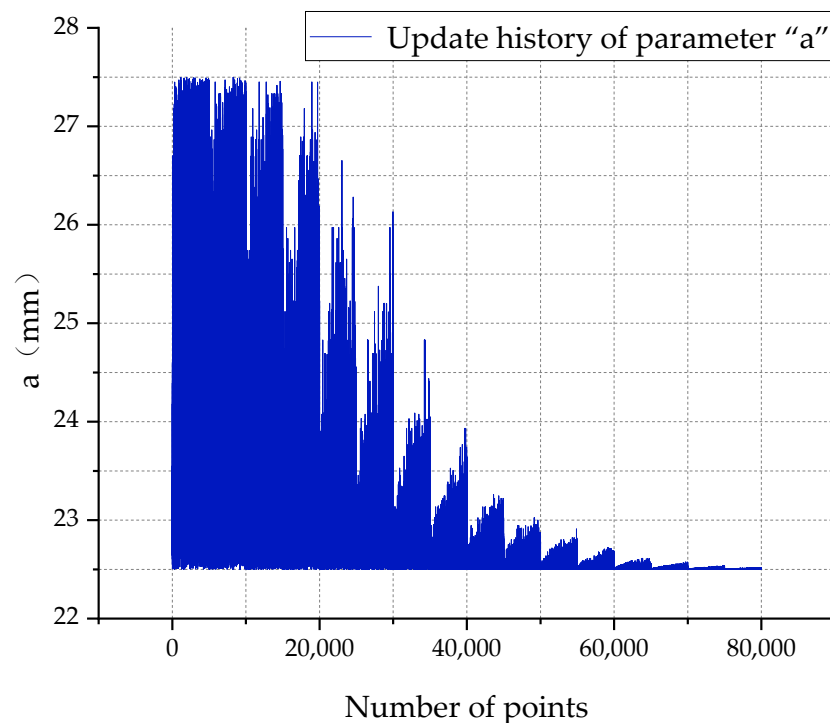

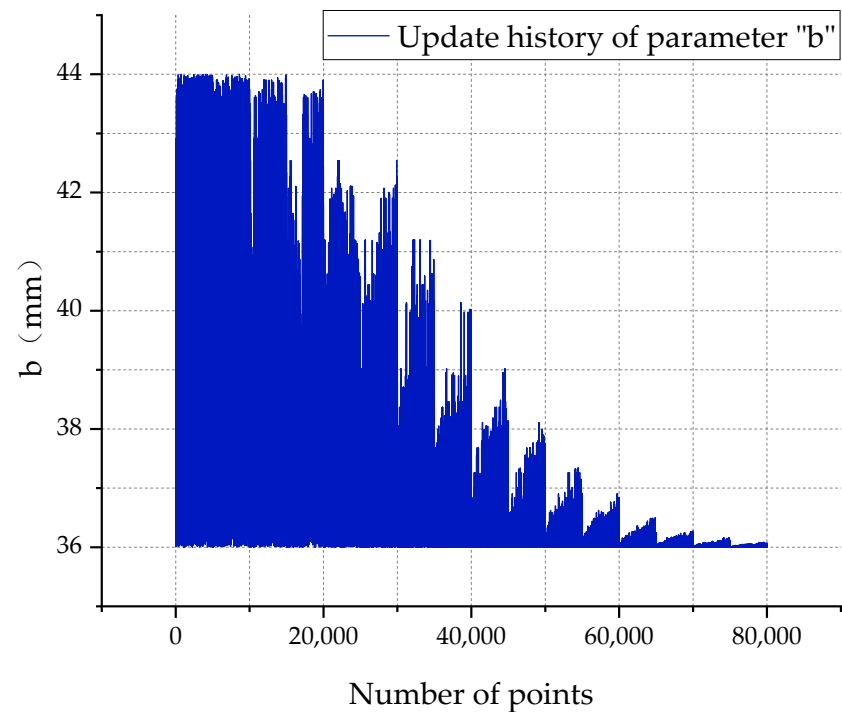**Figure 20.** The iterative process of parameter "a".

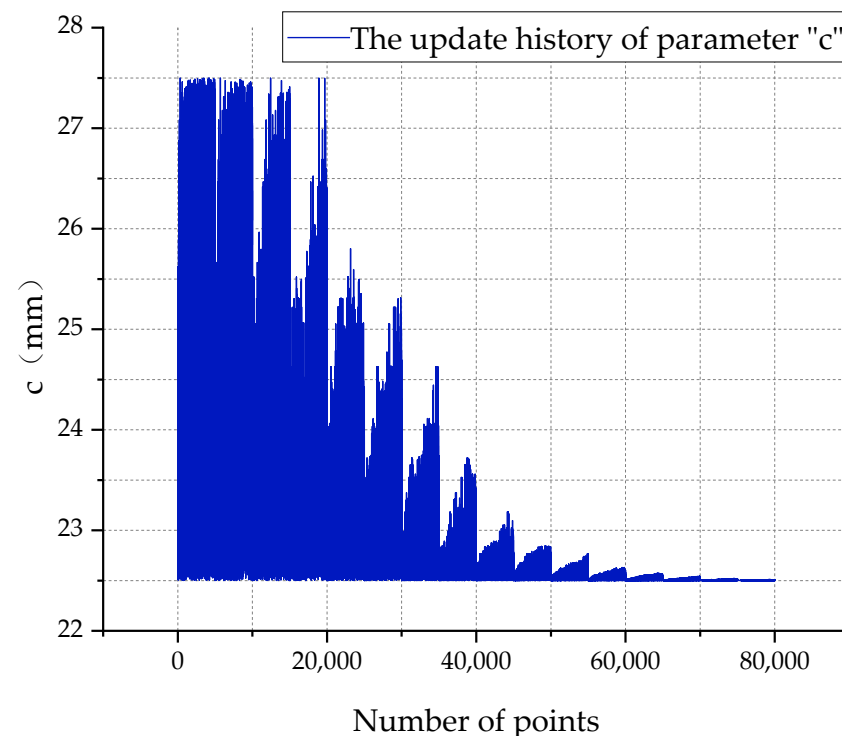**Figure 21.** The iterative process of parameter "b".

Figure 22. The iterative process of parameter "c".

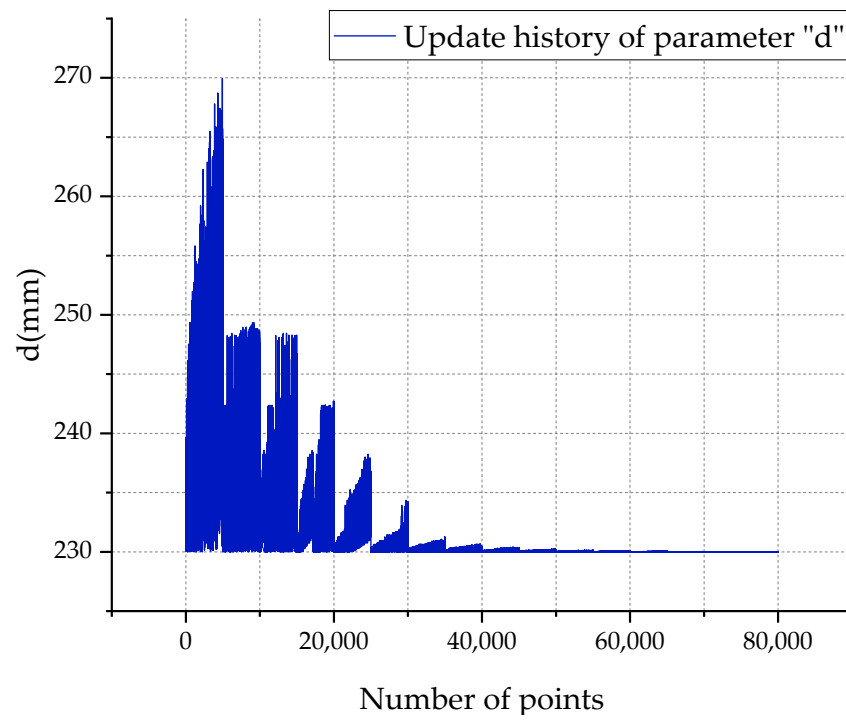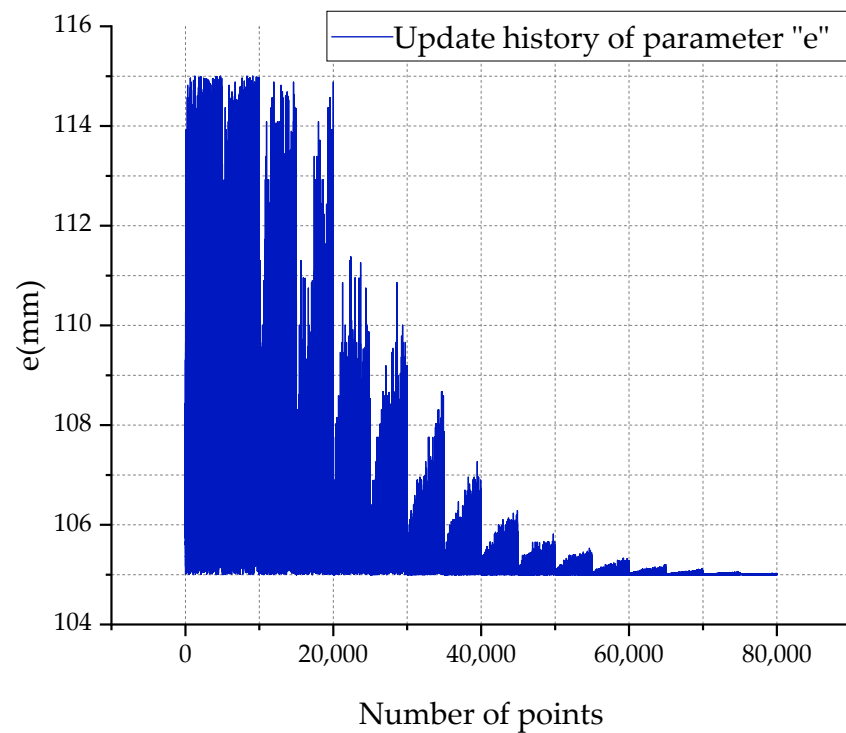**Figure 23.** The iterative process of parameter "d".

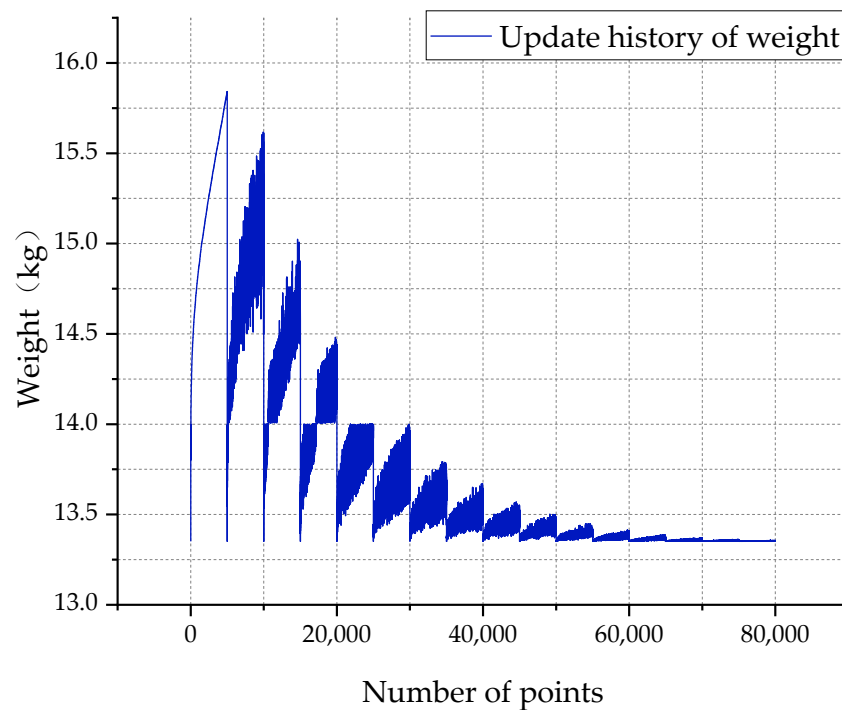**Figure 24.** The iterative process of parameter "e".

Figure 25. The iterative process of weight.

Figure 26. The iterative process of maximum deformation.

The optimization results show three optimal candidate points (Figure 27). Candidate point 3 is selected as the final result of optimization, and the results compare with the parameters before optimization (Table 4). The maximum deformation of the lightweight drive rod after optimization is reduced to one-tenth of that in original model 1/10 and the weight is reduced by 1.9 kg compared with original model.

Based on the above optimization results, the drive rod is remodeled according to the optimized parameters (Figure 28), and then finite element analysis is performed on it. Firstly, the material properties of QT900-2 are assigned to the remodeled lightweight

drive rod, and the model is meshed. After multiple verifications, accurate data can be obtained by controlling the mesh size to 4 mm (Figure 29). Finally, apply the die-cutting and inertia forces described in chapter 4.3 to the drive rod. After calculation, the strain and deformation of the optimized drive rod can be obtained (Figures 30 and 31).

Table of Schematic D4: Optimization							
	A	B	C	D	E	F	G
1	Optimization Study						
2	Minimize P9; 0 kg <= P9 <= 14 kg	Goal, Minimize P9 (Higher importance); Strict Constraint, P9 values between 0 kg and 14 kg (Higher importance)					
3	Minimize P7	Goal, Minimize P7 (Higher importance)					
4	Optimization Method						
5	MOGA	The MOGA method (Multi-Objective Genetic Algorithm) is a variant of the popular NSGA-II (Non-dominated Sorted Genetic Algorithm-II) based on controlled elitism concepts. It supports multiple objectives and constraints and aims at finding the global optimum.					
6	Configuration	Generate 5000 samples initially, 1000 samples per iteration and find 3 candidates in a maximum of 20 iterations.					
7	Status	Converged after 13556 evaluations.					
8	Candidate Points						
9		Candidate Point 1	Candidate Point 1 (verified)	Candidate Point 2	Candidate Point 2 (verified)	Candidate Point 3	Candidate Point 3 (verified)
10	P1 - a	22.64		22.636		22.722	
11	P2 - e	105.25		105.11		105.11	
12	P3 - d	41.207		40.32		40.756	
13	P4 - b	230.02		230.01		230.01	
14	P5 - c	24.215		24.313		24.159	
15	P7 - maximum deformation (mm)	-0.010154	0	-0.00997	0	-0.0098815	0
16	P9 - Weight (kg)	14.001	14	13.944	13.944	13.96	13.96

Figure 27. Optimization result drive rod.

Table 4. Parameter values of lightweight drive rod before and after optimization.

	a (mm)	b (mm)	c (mm)	d (mm)	e (mm)	Weight (kg)	Maximum Deformation (mm)
Before optimization	25	250	25	40	110	15.861	0.096997
After optimization	22.722	230.01	24.159	40.756	105.11	13.96	0.009882

According to the analysis results, the optimized drive rod mass is 13.352 kg, and the maximum deformation is 0.007514 mm (Table 5). Summarize and analyze the results of finite element analysis and optimization, and the results are consistent. Therefore, the optimization result of this time is reliable.

Table 5. Comparison between optimization results and mechanical verification results.

Parameter Name	Weight (kg)	Maximum Deformation (mm)
Optimization results	13.96	0.009882
Results of statics analysis	13.97	0.009768

Figure 28. Model after optimization.
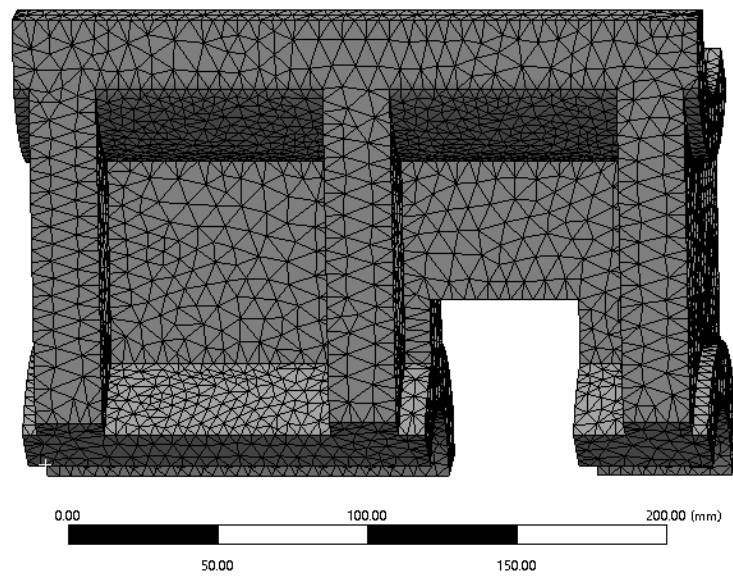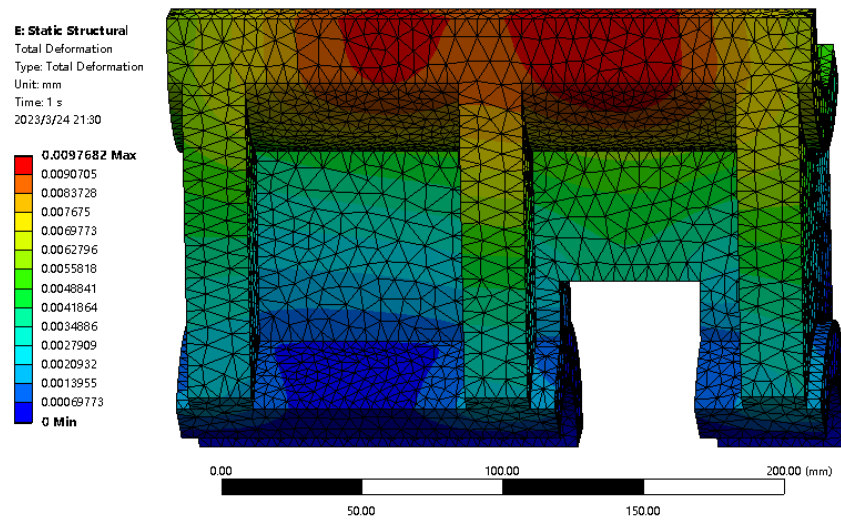
Figure 29. Grid division.
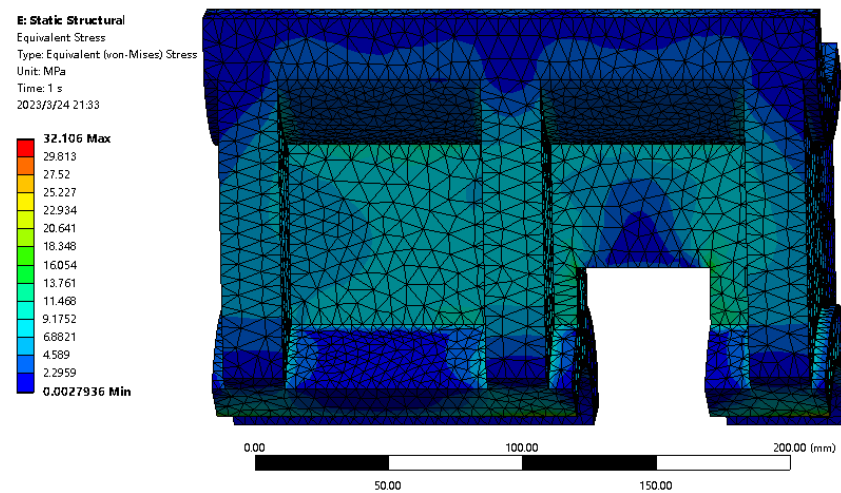

Figure 30. Deformation result.

Figure 31. Stress distribution result.

5. Dynamic Simulation of the Lightweight Drive Rod Based on Fully Symmetrical Structure in Die-Cutting Device Model

According to the above optimization results, the weight of the drive rod is smaller and the elastic deformation is smaller than before optimization. The finite element analysis of the optimized drive rod has been conducted above, verifying that the optimization results are accurate. As the drive rod is part of the die-cutting device, it is necessary to consider its deformation during assembly. Therefore, in order to obtain more accurate verification data, the drive rod is assembled in a die-cutting device for overall analysis to verify the specific deformation data of the lightweight drive rod in the assembly.

The optimized lightweight drive rod is matched in the assembly, assigning corresponding material properties to each part (Figure 32). The geometric structure is used to control the mesh quality, with a maximum mesh size of 50 mm and a minimum mesh size of 0.25 mm. Finally, 5,216,552 elements and 7,884,026 nodes are generated.

Figure 32. Meshing diagram of assembly.

Set the rotational speed of the crankshaft to 125 r/min, and then apply a 350t mold cutting force and the maximum inertial force acting on the drive rod on the upper surface of the mobile platform. According to the above settings, use ANSYS software to conduct dynamic simulation on the model of the die cutting device, and the simulation results are shown in Figure 33.

Figure 33. The deformation result diagram of the drive rod in the assembly.

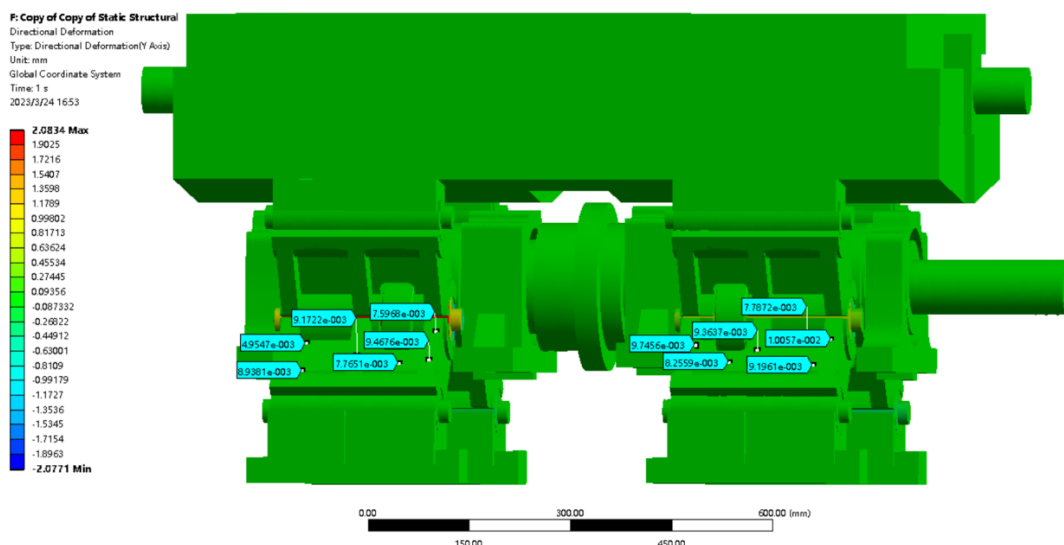According to the analysis results of the assembly, the deformation of each part of the optimized drive rod remains between 0.007 mm and 0.01 mm in the assembly. The verification results show that the optimization results are consistent with the simulation results. Therefore, the optimization design of the lightweight drive rod in this study meets the target requirements and provides an optimized structure for the optimization and upgrading of the die-cutting device.

After the above mechanical verification of the designed drive rod, relevant enterprises put the drive rod into production trial. Figure 34 shows the application diagram of the designed lightweight drive rod assembled in real objects.
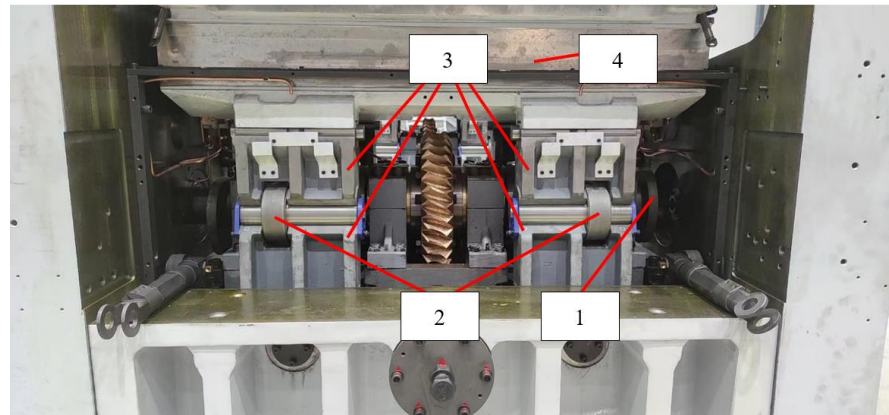

Figure 34. Application diagram of fully symmetrical lightweight drive rod. 1-crankshaft; 2-power rod; 3-lightweight drive rod; 4-moving platform.

Through the trial and commissioning of enterprises, after the application of the lightweight drive rod designed in this paper, the die-cutting device can still maintain high-precision die-cutting under the working conditions of high speed and high die-cutting force. Due to the limited conditions, it is temporarily impossible to measure the inertia force and deformation of the lightweight drive rod in the prototype directly, so we should check it from another angle. According to the operation of the prototype, when the die-cutting device operates at the maximum die-cutting force of 350t and the high speed of 125 r/min, its stability has been significant improved, and it can still achieve higher die-cutting accuracy. Therefore, it can be considered that the actual operation of the lightweight drive rod in this study is basically consistent with the design goal, achieving the design goal.

6. Conclusions

(1) According to the force distribution of drive rod and the principle of structural mechanics, a lightweight drive rod based on fully symmetrical structure is proposed. From the comparison of the mechanical properties of the designed drive rod, compared with the traditional double-elbow bar, the maximum elastic deformation of the drive rod under the working conditions is reduced from 0.303 mm to 0.096 mm, and the overall weight of the drive rod is reduced from 21.93 kg to 15.86 kg. It can be concluded that the strength of the drive rod has been significantly improved, and a lightweight design has been achieved, which is conducive to improving die cutting accuracy.

(2) The structural parameters of the drive rod are further optimized using the Non-dominated Sorting Genetic Algorithm-II (*NSGA-II*), and the optimized deformation and weight of the drive rod are obtained through finite element analysis. The validation results are consistent with the optimization results. After parameter optimization, the maximum deformation of the drive rod under working condition is reduced from 0.096 mm to 0.0098 mm, and the total weight is reduced from 15.86 kg to 13.96 kg. The results show that the mechanical and kinematic performance of the optimized lightweight drive rod has been further improved.

(3) Finally, a lightweight driving rod is applied to the model of a die cutting device, and the elastic deformation of the driving rod is verified through dynamic simulation. The maximum deformation of the drive rod in the die-cutting device is kept between 0.007~0.01 mm, which is consistent with the previous optimization results. Through the verification and comparison of the above results, the performance of the lightweight drive rod has reached the expected research goal. Therefore, this study provides practical guidance for lightweight drive rods. If subsequent conditions permit, the team will continue to test the die cutting accuracy and stability of the physical prototype.

Author Contributions: J.W. conceived the scheme and designed the structure, collected and analyzed the data, and wrote and revised a paper; Y.L. conceived the scheme and designed the structure, proposed the optimization method, and revised the paper. X.C. simulation analysis, the results verified. All authors have read and agreed to the published version of the manuscript.

Institutional Review Board Statement: Not applicable.

Informed Consent Statement: Not applicable.

Data Availability Statement: Not applicable.

Conflicts of Interest: The authors declare no conflict of interest.

Nomenclature

l_1	The lengths of OA, $l_1 = 45$ mm
l_2	The lengths of AB, $l_2 = 217$ mm
l_3	The lengths of BC, $l_3 = 178$ mm
l_4	The lengths of CD, $l_4 = 280$ mm
l_5	The lengths of DO, $l_5 = 185.3$ mm
φ_1	The position angle of OA
φ_2	The position angle of AB
φ_3	The position angle of BC
ω_1	The angular velocities of OA, $\omega_1 = 125$ r/min
ω_2	The angular velocities of AB
ω_3	The angular velocities of BC
a_2	Angular acceleration of AB
a_3	Angular acceleration of BC
F'	Strength value of inertia force of drive rod
a_i	The value of the angular acceleration of the drive rod
m	The weight of the drive rod
J	Moment of inertia of drive rod
r_T	Rotation radius of drive rod
$a, b, c, d,$ e, f, g, r	These are the size parameters 1, 2, 3, 4, 5, 6, 7 and 8 of the drive rod, as shown in Figure 13
R, h, θ	These are the size parameters 9, 10 and 11 of the drive rod, as shown in Figure 17
F_N	The maximum die-cutting force component on one of the drive rods
L	The length of the lightweight drive rod, namely the value of "b"
E	Elastic modulus of drive rod
A	Cross-sectional area of drive rod in axial direction
ρ	Density of drive rod
F_Σ	The sum of the axial components of the maximum die-cutting force and the maximum inertia force on the drive rod
F'_{max}	Axial component of the maximum inertia force on the drive rod

References

1. Ternytskyi, S.; Rehei, I.; Kandiak, N.; Radikhovskyi, I.; Mlynko, O. Experimental Research of Paperboard Cutting in Die Cutting Press with the Screw–Nut Transmission of Drive Mechanism of a Movable Pressure Plate. *Acta Mech. Autom.* **2021**, *15*, 122–131. [CrossRef]
2. Lian, G.; Yao, M.; Zhang, Y.; Huang, X. Analysis and Respond Surface Methodology Modeling on Property and Performance of Two-Dimensional Gradient Material Laser Cladding on Die-cutting Tool. *Materials* **2018**, *11*, 2052. [CrossRef] [PubMed]
3. Ye, S.; Qu, F.K. A Simple Automatic Die-cutting Machine Design. *Mod. Manuf. Technol. Equip.* **2021**, *57*, 118–119. [CrossRef]
4. Xu, H.W.; Huang, J.C.; Chen, L.L.; Dong, J.Z. Research on Registration Algorithm of Plane Digital Die-cutting Based on Visual Image. In Proceedings of the 2022 IEEE 5th International Conference on Information Systems and Computer Aided Education (ICISCAE), Dalian, China, 23–25 September 2022; IEEE: Dalian, China, 2022; pp. 84–87.
5. Wang, K.J.; Lee, Y.H.; Angelica, S. Digital Twin Design for Real-time Monitoring—A Case Study of Die-cutting Machine. *Int. J. Prod. Res.* **2021**, *59*, 6471–6485. [CrossRef]
6. Huang, C.T.; Lin, H.H.; Su, C.H. Polygonal Object Dilation and Packing in Vector Space for Die-cutting Machine Tools. In Proceedings of the 2017 International Conference on Applied System Innovation (ICASI), Sapporo, Japan, 13–17 May 2017; IEEE: Sapporo, Japan, 2017; pp. 1793–1796.
7. Wu, T. Application and Development of New Technology of Automatic Die-cutting Machine. *New Type Ind.* **2022**, *12*, 268–271. [CrossRef]
8. Knysh, O.; Rehei, I.; Kandiak, N.; Ternytskyi, S.; Ivaskiv, B. Experimental Evaluation of Eccentric Mechanism Power Loading of Movable Pressure Plate in Die-Cutting Press. *Acta Mech. Autom.* **2022**, *16*, 266–273. [CrossRef]
9. Lin, W.G.; Zhou, C.; Huang, W.J. Optimum Design for Mechanical Structures and Material Properties of the Dual-Elbow-Bar Mechanism. *Adv. Mater. Sci. Eng.* **2015**, *2015*, 724171. [CrossRef]
10. Luo, Y.; Cheng, G.H. Elastic Statics Analysis of the Linkage Mechanism in Die-cutting Machine. *Light Ind. Mach.* **2008**, *26*, 29–31.
11. Yu, Q.; Weng, Z.M. Computer Emulating of the Dual-elbow-bar Mechanism of the Die-cutting Machine. *Packag. Eng.* **2006**, *27*, 191–193.
12. Zhang, X.S.; Chai, S.Z.; Cheng, G.H.; Li, J.Y. Motion Analysis and Optimum Design of the Dual-elbow-bar Mechanism of the Die-cutting Machine. *Beijing Inst. Graph. Commun.* **2006**, *2*, 32–34. [CrossRef]
13. Lv, F.M. Design and Kinematics of a New Intermittent Mechanism of Die-cutting Machine. *Packag. Eng.* **2020**, *41*, 204–209. [CrossRef]
14. Xie, J.G.; Zou, H.J. Dynamic Analysis of the Double-elbow-bar Mechanism of Automatic Vertical Platen Die-cutter. *Mechane Des. Res.* **2005**, *21*, 75–78.
15. Wei, Y.B.; Zhao, Q.H.; Zhang, H.Y. Characteristic Research of Elbow-bar Framework of Blocking Die-cutter. *Mach. Des. Res.* **2005**, *21*, 76–78. [CrossRef]
16. Nu, N.; Cai, J.F.; Zhang, Y. Analysis and Research on Driving Mechanism of Die-cutting Mobile Platform. *Beijing Print. Inst.* **2018**, *26*, 6–9. [CrossRef]
17. Nu, N.; Han, X.; Wang, Q.F.; Cai, J.F.; Zhang, Y. Analysis and Research on the Cam of the Transmission System of Die cutting Machine. *Green Package* **2018**, *6*, 49–52. [CrossRef]
18. Xiao, J. Analysis and Influence Study on Geometric Error of Main Cutting Mechanism of Flat Die Cutter. Ph.D. Thesis, Xi'an University of Technology, Xi'an, China, 2016.
19. Huang, W.T.; Wu, J.M.; Liu, L.J. Analysis of Factors Affecting the Accuracy of Die-cutting Machine. *Print. Mag.* **2009**, *11*, 57–60.
20. Song, S.N. Discussion on the Factors Affecting the Accuracy of Die-cutting Machine. *Innov. Appl. Sci. Technol.* **2016**, *20*, 100.
21. Shen, S.H.; Shi, X.D.; Yuan, Y.C. Optimal Design of Conjugate Cam-linkage Combined Mechanism for Pressure Device in Die-cutting. In *Applied Mechanics and Materials*; Trans Tech Publications Ltd.: Beijing, China, 2012; Volume 120, pp. 178–181. [CrossRef]
22. Zhang, Y.; Make, X.; Qi, Y.; Cheng, Q. Die-Cutting Pressure Detection Analysis Based on TRIZ Theory and Simulation. In Proceedings of the 2021 3rd International Conference on Artificial Intelligence and Advanced Manufacture, Manchester, UK, 23–25 October 2021; pp. 720–723. [CrossRef]
23. Jiao, L.Q.; Wang, Y.M.; Wu, S.Q.; Li, L.H. Study on Pressure Testing Method of Die-Cutting Machine Based on Micro-capsule and Image Sensor. In Proceedings of the ICMEIT 2018, Shanghai, China, 15–16 April 2018; pp. 32–38.
24. Shi, X.D.; Li, Y.; Li, H.D. Analysis of Platen Die-Cutting Mechanism Based on the Axiomatic Design Theory. In *Applied Mechanics and Materials*; Trans Tech Publications Ltd.: Beijing, China, 2013; Volume 312, pp. 796–799.
25. Shen, Y.S. *Mechanical Principles Tutorial*; Tsinghua University Press: Beijing, China, 2015; Volume 33–66, pp. 296–320.
26. Liu, H.W. *Mechanics of Materials I*; Higher Education Press: Beijing, China, 2017; pp. 13–51.
27. Jiang, W.; Xie, W.; Sun, S. Parametric Optimisation Analysis of Micro/Nano-Satellite Flywheels Based on the NSGA-II Optimisation Algorithm. *Aerospace* **2022**, *9*, 386. [CrossRef]

28. Liu, Y.; Yan, C.; Ni, H.; Mou, Y. Multi-objective Optimization Decision of High-speed Dry Hobbing Process Parameters Based on GABP and Improved NSGA-II br. *China Mech. Eng.* **2021**, *32*, 1043. [CrossRef]

29. Zhao, W.G.; Xia, T.; Sheng, Y.Z.; Li, S.S. Multi-objective Parameters Optimization of Low Specific Speed Centrifugal Pump Based on NSGA-II Genetic Algorithm. *J. Lanzhou Univ. Technol.* **2020**, *46*, 55.